15th Australasian Wind Engineering Society (AWES) Workshop
Sydney, Australia
23-24 February, 2012

Bifurcation Prediction of the Aeroelastic Galloping Model with Structural and Damping Non-Linearities

G. A. Vio[1]

[1]School of Aerospace, Mechanical and Mechatronic Engineering
University of Sydney, Sydney, NSW 2006, Australia

Abstract

A global stability analysis of the transverse galloping of a square section oscillator in a normal steady flow was implemented. The analysis is applied to a mathematical model using experimentally determined stationary aerodynamic forces. The model is an ordinary differential equation with small non-linearity in the velocity term. A number of stability analysis methods will be compared. The resulting stability predictions are compared with each other and with results obtained from numerical integration. It is shown that the non-linear aeroelastic oscillator presents hysteretic stability over a range of wind speeds. All methods had varying degree of success on capturing the bifurcation behaviour of the aeroelastic oscillator.

Introduction

Recent interest in non-linear aeroelastic problems has resulted in a number of very detailed aeroelastic simulations combining Finite Element solutions for the structure and Computational Fluid Dynamic solutions for the aerodynamic forces, e.g. Girodroux-Lavigne and Dugeai (2003). However, such calculations are extremely computationally expensive. Furthermore, the determination of the stability of such systems requires the repetition of these calculations at various wind speeds and from various initial conditions. Therefore, stability prediction from CFD-FE calculations is prohibitively time-consuming. An alternative is the application of local linearisation methods in order to predict the bifurcation points, e.g. Badcock et al (2003), usually after performing some type of model order reduction (Silva et al (2003)). Various such linearisation methods have been proposed, holding varying degrees of promise. There are several forms of aeroelastic behaviour associated with bluff bodies. The best known is vortex excited oscillation, in which a body vibrates in a particular mode over a small discrete range of wind speed containing the speed at which the shedding frequency of the Von Karman Vortex Street formed in the wake coincides with the natural frequency of the mode. Almost as well known are the forms generally called galloping, which have in common the fact that the cylinder cross sections are aerodynamically unstable, so that the small amplitude vibrations generate forces which increase the amplitudes to large values. The form of the motion is pure translational in the direction normal to the plane of the incident wind and the cylinder axis.

Galloping is defined as an instability typical of slender structures (Simiu and Scanlan (1986)). It is a relatively low-frequency oscillatory phenomenon of elongated, bluff bodies acted upon by a wind stream. The frequency at which the bluff object responds is much lower than the frequency of vortex shedding. It is in this sense that galloping may be considered as a low frequency phenomenon. There are two types of galloping: wake and across-wind Scruton (1960).

- Wake galloping. This effect occurs when two cylinders are present, where one is upstream, producing a wake, and one downstream, within that wake, and the cylinders are separated by a distance of few diameters (fig. 1). In this type of flow the downstream body is subjected to galloping oscillations induced by the turbulent wake of the upstream cylinder. Consequently, the upstream cylinder tends to rotate clockwise while the downstream cylinder rotates in anti-clockwise motion, inducing torsional oscillations.

- Across-wing galloping. This effect occurs when the wind blows transversely across an object, such as a bridge deck. This type of instability causes a crosswise vibration of the object. As the object vibrates in a steady wind velocity, the relative velocity changes, thereby changing the angle of attack (α). Due to this change in incidence, an increase or decrease in lift force on the cylinder occurs. If an increase in α causes an increase in the lift in the opposite direction of motion, the oscillation is stable. On the other hand if the opposite occurs, i.e. an increase of α causes a decrease in lift force, then the oscillation is unstable and galloping occurs (fig. 2). A classical example of this phenomenon is observed in ice covered power transmission lines. Generally galloping is avoided by reducing the distance between the supports and increasing the tension of the lines.

Many researchers have studied the instability mechanism in the flow over a square cylinder, which gives rise to galloping vibration Parkinson and Brooks (1961); Parkinson and Smith (1964); Bearman and Luo (1988); Blevins (1990). The quasi-steady theory was first presented in Parkinson and Brooks (1961) where a fifth order polynomial non-linearity was introduced to describe the aerodynamic force. This formulation was later developed in Parkinson and Smith (1964) by extending the approximation up to seventh order. This new approximation allows for an accurate representation of the point of inflection, thus making it possible for the hysteresic phenomenon to appear. This phenomenon was not observed in the original study by Parkinson Parkinson and Brooks (1961). The relationship between point of inflection and the existence of a hysteretic loop was proven in Luo et al (2003). In Norberg (1993) a dependency between Reynolds number and hysteresis was found experimentally. The validity of quasi-steady theory was investigated in Bearman and Luo (1987) and Bearman and Luo (1988) at different damping levels and reduced frequencies. It is important to note that, for bluff bodies, at low reduced velocity both galloping and vortex-induced vibration can occur. It was concluded that quasi-steady theory is valid as long as the critical reduced velocity is four times the reduced velocity at which vortex resonance occurs. Investigation into the complex behaviour between vortex resonance and galloping was performed in Parkinson and Wawzonek (1981). Galloping instability has been the subject of very little research using numerical simulation. Recently the influence of damping and the effect of aspect ratio was investigated Robertson et al (2003). The effects on the galloping oscillation are compared with the quasi-steady results

obtained in earlier work Parkinson (1971).

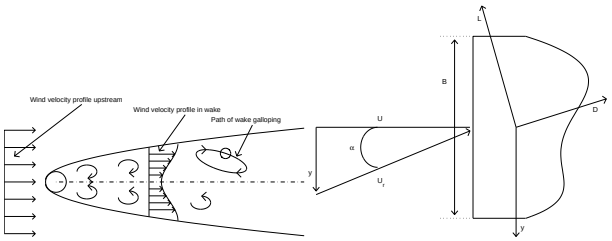

Figure 1: Wake galloping model

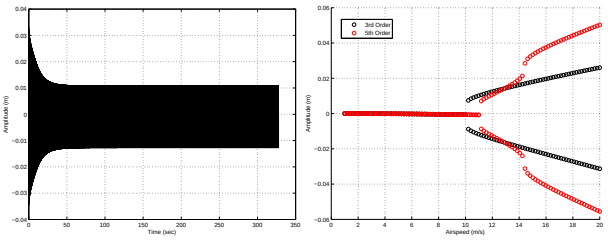

Figure 2: Effect of across wind galloping on lift force

Aeroelastic Galloping Model

The aeroelastic galloping model is modelled as a mass with linear stiffness and non-linear damping as shown in fig. 3. In this study the model derived in Andrienne and Dimitriadis (2011) will be used. The following expression was used to model the wind tunnel experimental data

$$m\ddot{y}+c\dot{y}+ky+\tfrac{1}{2}\rho V_\infty bA_1\dot{y}+\tfrac{1}{2}\rho bA_2\dot{y}|\dot{y}|+\tfrac{1}{2V_\infty}\rho bA_3\dot{y}^3+$$

$$\tfrac{1}{2V_\infty^2}\rho bA_4\dot{y}^3|\dot{y}|+\tfrac{1}{2V_\infty^3}\rho bA_5\dot{y}^5=-\tfrac{1}{2}\rho V_\infty^2 bc_l(\alpha_0) \quad (1)$$

The A_i coeffients are derived by curvitting of the experimental data. The values are listed in table 1. m, c, k are the mass, damping and stiffness coefficient respectively. b is the body chord length and ρ the air density.

A_0	4.10×10^{-1}	A_3	1.42×10^{4}
A_1	-1.65	A_4	-2.67×10^{5}
A_2	-2.6850×10^{2}	A_5	$1.69e\times10^{6}$

Table 1: Experimental Value of curvefitted data - 5^{th} order

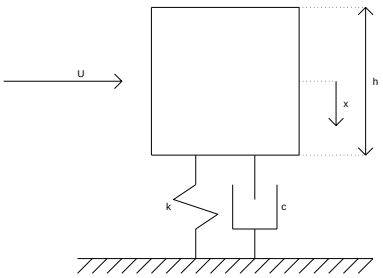

Figure 3: Aeroelastic galloping model

The most accurate solution of the galloping equation of motion 1 can be obtained through numerical integration. A number of methods exist for integrating such equations of motion. For this work the Matlab and Simulink ODE suite is used and more specifically the ODE45 routine which is based on an explicit Runge-Kutta (4,5) formula, the Dormand-Prince pair Dormand and Prince (1980). A sample resposne at 12 m/s is shown in figure 4. It can be seen that the response settles to a LCO of amplitude 0.011 after 50 seconds. Plots such as figure 4 are not practical for obtaining a description of the global behaviour of the system. Bifurcation diagrams can then be used to plot global results. A bifurcation diagram is obtained by plotting the maxima of the steady-state response of the system at each airspeed and for every set of initial conditions (essentially, it is a series of Poincaré plot). Figure 5 presents the bifurcation plot for the system as given in equation 1. The figure compares the same system when a 3^{rd} and 5^{th} order approximation of the system under investigation i utilised. Both approximation capture the initial jump in amplitude, due to a fold bifurcation, has the non-linear terms start to have an effect and a stable limit cycle is created. A second jump occurs at around 14 m/s, and this is captured by the 5^{th} order approximation.

Figure 4: Galloping response at 12 m/s

Figure 5: Bifurcation plot

Structural and Damping Non-Linearities

Non-linearities appear in all system and can have a significant effect on the resposne of a system. Here two types of non-linearities will be introduced, namely a free-play non-linearity, eqution 2, and a Coulomb frictinon-linearity (equation 3. Typical restoring force graphs are shown in figure 6.

$$M(x)=\begin{cases} kx+k\delta\text{sgn}(x) & |x|\geq\delta \\ 0 & |x|<\delta \end{cases} \quad (2)$$

where δ is the size of the free-play region and sgn is the signum function. The Coulomb non-linearity can be expressed as follows

$$G(\dot{x})=c\dot{x}+\mu F_n\text{sgn}(\dot{x}) \quad (3)$$

where μ is the coefficient of friction and F_n the normal force.

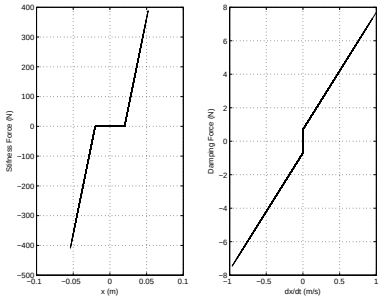

Figure 6: Restoring Force

Prediction Method

Harmonic Balance

The harmonic balance presented is based on the formulation of Yang and Zhao (1988) and McIntosh et al (1981). The main assumption of this technique is to assume that the system admits a sinusoidal limit cycle and, hence, its response is given by $y=Ysin(t)$ and $\dot{y}=Ycos(t)$, where Y is the limit cycle amplitude. Then, using a Fourier Serie expansion of the non-linear forces in the system, the non-linearities are replaced by equivalent linear stiffness and damping terms. For example, consider the equation of motion of a general single degree of freedom system,

$$m\ddot{x}+c\dot{x}+kx+f_{nl}(x,\dot{x})=0 \quad (4)$$

After applying the Harmonic Balance method, the non-linear term is replaced by a sum of linear terms

$$f_{nl}(x,\dot{x}) = K_{eq}x + C_{eq}\dot{x} \tag{5}$$

where K_{eq} and C_{eq} are the equivalent linear stiffness and damping terms respectively. From eq. 1 it can be noted that only non-linear damping is present in the galloping problem, given by

$$\begin{aligned} f(\dot{y}) = {} & \tfrac{1}{2}\rho V_\infty b A_1 \dot{y} + \tfrac{1}{2}\rho b A_2 \dot{y}|\dot{y}| + \tfrac{1}{2V_\infty}\rho b A_3 \dot{y}^3 + \\ & \tfrac{1}{2V_\infty^2}\rho b A_4 \dot{y}^3|\dot{y}| + \tfrac{1}{2V_\infty^3}\rho b A_5 \dot{y}^5 - \tfrac{1}{2}\rho V_\infty^2 b c_l(\alpha_0) \end{aligned} \tag{6}$$

This non-linear term can be expanded as a Fourier series, as follows

$$f(\dot{y}) = \frac{a_0}{2} + \sum_{n=1}^{\infty} a_n \cos(nt) + \sum_{n=1}^{\infty} b_n \sin(nt) \tag{7}$$

where the a_n and b_n coefficients are given by

$$\begin{aligned} a_o &= \tfrac{1}{\pi}\int_0^{2\pi} f(\dot{y})dt \\ a_n &= \tfrac{1}{\pi}\int_0^{2\pi} f(\dot{y})cos(nt)dt \\ b_n &= \tfrac{1}{\pi}\int_0^{2\pi} f(\dot{y})sin(nt)dt \end{aligned} \tag{8}$$

For a first order Harmonic Balance calculation only the first harmonic term is considered, thus only requiring the first term of the Fourier expansion. Assuming that $y = Ysin(t)$ and $y' = Ycos(t)$, the Fourier coefficients become

$$\begin{aligned} a_o &= \tfrac{1}{\pi}\int_0^{2\pi} f(Ycos(t))dt \\ a_n &= \tfrac{1}{\pi}\int_0^{2\pi} f(Ycos(t))cos(nt)dt \\ b_n &= \tfrac{1}{\pi}\int_0^{2\pi} f(Ycos(t))sin(nt)dt \end{aligned} \tag{9}$$

and after performing the intergration the following expression is obtained

$$C_{eq} = \frac{1}{2}\rho b\left\{\frac{5A_5}{8V_\infty^3}Y^4 + \frac{32A_4}{15\pi V_\infty^2}Y^3 + \frac{3A_3}{4V_\infty}Y^2 + \frac{8A_2}{3\pi}Y + V_\infty A_1\right\} \tag{10}$$

thus yielding the following equation for an equivalent linearised system

$$\begin{aligned} & m\ddot{y} + c\dot{y} + ky + \tfrac{1}{2}\rho b \\ & \left\{\tfrac{5A_5}{8V_\infty^3}Y^4 + \tfrac{32A_4}{15\pi V_\infty^2}Y^3 + \tfrac{3A_3}{4V_\infty}Y^2 + \tfrac{8A_2}{3\pi}Y + V_\infty A_1\right\} = 0 \end{aligned} \tag{11}$$

This equation was derived using the assumption that $y = Y\sin(t)$. Substituting this value yields

$$\begin{aligned} & \left[\tfrac{5A_5}{8V_\infty^3}Y^4 + \tfrac{32A_4}{15\pi V_\infty^2}Y^3 + \tfrac{3A_3}{4V_\infty}Y^2 + \tfrac{8A_2}{3\pi}Y + V_\infty A_1 + \tfrac{2c}{\rho b}\right] \\ & \tfrac{1}{2}\rho b Y\cos(t) = 0 \end{aligned} \tag{12}$$

or for a non-trivial solution (i.e. $Y \neq 0$)

$$\frac{1}{2}\rho b\left\{\begin{array}{l} \tfrac{5A_5}{8V_\infty^3}Y^4 + \tfrac{32A_4}{15\pi V_\infty^2}Y^3 + \tfrac{3A_3}{4V_\infty}Y^2 + \\ \\ \tfrac{8A_2}{3\pi}Y + V_\infty A_1 + \tfrac{2c}{\rho b} \end{array}\right\} = 0 \tag{13}$$

Equation 13 can be solved for the amplitude Y of all the possible limit cycle at each given airspeed. The solution of the equation can be real or complex conjugate pairs. Only the solutions that yield real and positive amplitudes are considered, all others are ignored. Figure 7 compares the solution of the

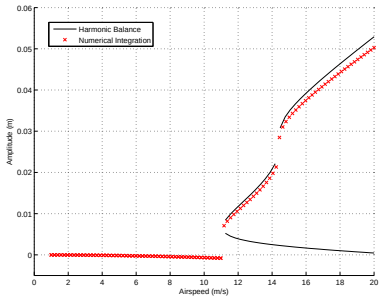

Figure 7: Harmonic Balance Result

Harmonic Balance method against the numerical integration results. The harmonic balance methods predict accurately the amplitude of the stable limit cycle. A boundary of unstable limit cycle is also predicted, which would be in line with experimental results, which show the existance of low amplitude limit cycles Andrienne and Dimitriadis (2011).

Results

The effect of the non-linearities on the response of the system is shown in figures 8-10. Here the freeplay region δ is set to 0.01 radians and the Coulomb damping to 10% of the linear viscous damping. The presence of the damping non-linearity has a beneficial effect on the overall response of the system (figure 8). The start of the bifurcation is delayed by over 5 m/s. This is expected as the linearised form of eq. 3 is

$$f_{nl}(x,\dot{x}) = \frac{4\mu F_n x}{A\pi} + c\dot{x} \tag{14}$$

Adding Coulomb friction increases proportionally the value of the damping present within the system. The limit cycle amplitude grows much more quickly and tends to converges to the same amplitude limit cycle as the model with only aerodynamic non-linearity present. The addition of a free-play non-linearity has a minimal effect on the response, as shown in figure 9. The location of the bifurcation is at the same airspeed, as the stiffness does not influence the location of the bifurcation point. The linearised form of the free-play non-linearity (eq. 2), becomes

$$f(x,\dot{x}) = \frac{k}{\pi}x(pi - 2t_1 - sin(2t_1)) \tag{15}$$

where $t_1 = asin(\delta/A)$ and A is the assumed limit cycle amplitude. The amplitude of the limit cycle is increased and the increase is constant throughout the airspeed region. When both non-linearities are present the behavior of the system is changed dramatically (figure 10). The delay in the start of the bifurcation is still present from the Coulomb non-linearity with a quick growth in limit cycle amplitude as the airspeed is increased. The limit cycle ampltitude then grows beyond that of the original model. The major difference been a shift in the steady-state value of the response at low airspeed. Here the response settles to a value of $-\delta$, thus creating an initial asymmetric limit cycle. As the airspeed is increased the limit cycle becomes symmetric again. This effect is due to the friction component proportional to the displacement which forces the response to decay at one of the newly generated equilibrium points of the limit cycle, namely the turning point of the free-play non-linearity.

Conclusions

This paper has shown the difficulty in predicting the behaviour of a simple aeroelastic system, in this case an aeroelastic galloping model. Non-linearities have a major effect in determining the response of the model, and combination of these non-linearities can lead to different steady-state conditions that need

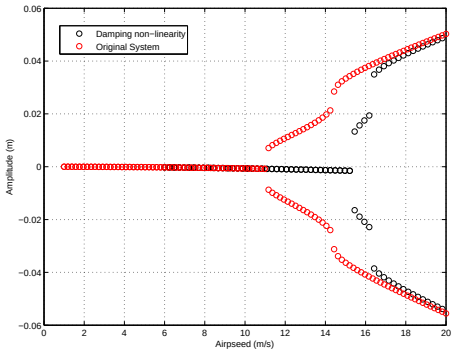

Figure 8: Numerical Integration Results - Damping non-linearity

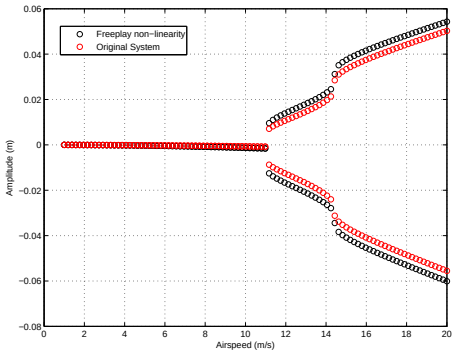

Figure 9: Numerical Integration Results - Stiffness non-linearity

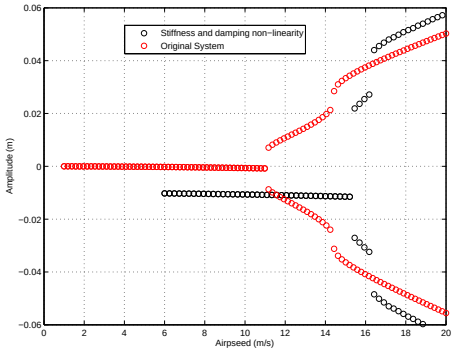

Figure 10: Numerical Integration Results - Damping and Stiffness non-linearity

to be accounted for. Non-linearities can have a beneficial effect in delaying the potentially dangerous condition of limit cycle oscillations, as is the case with Coulomb friction. Free-play non-linearity has an overall detrimental effect to the response.

*

References

Andrienne T, Dimitriadis G (2011) Experimental analysis of the bifurcation behaviour of a bridge deck undergoing across-wind galloping. In: Proceedings of the 8^{th} International Conference on Structural Dynamics, Leuven, Belgium

Badcock K, Woodgate M, Richards B, Barakos G (2003) The application of sparse matrix techniques to the cfd based bifurcation analysis of a symmetric wing. In: Proceedings of the CEAS International Forum on Aeroelasticity and structural dynamics, Amsterdam, The Netherlands

Bearman P, Luo S (1987) Experiments on flow induced vibration of a square-section cylinder. Journal of Fluids and Structures 1:19–34

Bearman P, Luo S (1988) Investigation of the aerodynamic instability by forced oscillation. Journal of Fluids and Structures 2:161–176

Blevins R (1990) Flow induced vibration, 2nd edn. Van Nostrand Reinhold, New York

Dormand JR, Prince PJ (1980) A family of embedded Runge-Kutta formulae. Journal of Computational and Applied Mathematics 6:19–26

Girodroux-Lavigne P, Dugeai A (2003) Transonic aeroelastic computations using navier-stokes equations. In: Proceedings of the CEAS International Forum on Aeroelasticity and structural dynamics, Amsterdam, The Netherlands

Luo S, Chew Y, Ng Y (2003) Hysteresis phenomenon in the galloping oscillation of a square cylinder. Journal of Fluids and Structures 18:103–118

McIntosh S, Reed R, Rodden W (1981) Experimental and theoretical study of nonlinear flutter. Journal of Aircraft 18(5):1057–1063

Norberg C (1993) Flow around rectangular cylinders-pressure and wake frequencies. Journal of Wind Engineering and Industrial Aerodynamics 49:187–196

Parkinson G, Wawzonek M (1981) Some considerations of combined effects of galloping and vortex resonance. Journal of Wind Engineering and Industrial Aerodynamics 8:135–143

Parkinson GV (1971) Wind-induced instability of structures. Philosophical Transactions of the Royal Society of London A269:395–409

Parkinson P, Brooks N (1961) On the aeroelastic instability of bluff cylinders. Journal of Applied Mechanics 28:252–258

Parkinson P, Smith JD (1964) The square prism as an aeroelastic non-lnear oscillator. Quarterly Journal of Mathematical and Applied Mathematics 17(2):225–239

Robertson I, Li L, Sherwin S, Bearman P (2003) A numerical investigation of rotational and transverse galloping rectangular bodies. Journal of Fluids and Structures 17:681–699

Scruton C (1960) The use of wind tunnel in industrial research. Tech. Rep. 309, AGARD

Silva WA, Hong MS, Bartels RE, Piatak DJ, Scott RC (2003) Identification of computational and experimental reduced-order models. In: Proceedings of the CEAS International Forum on Aeroelasticity and structural dynamics, Amsterdam, The Netherlands

Simiu E, Scanlan R (1986) Wind effect on strucutres, 3rd edn. Wiley Interscience

Yang ZC, Zhao LC (1988) Analysis of limit cycle flutter of an airfoil in incompressible flow. Journal of Sound and Vibration 123(1):1–13